Reactivity, Secondary Structure, and Molecular Topology of the *Escherichia coli* Sulfite Reductase Flavodoxin-like Domain†

Ludovic Champier,[‡,§] Nathalie Sibille,[§,||] Beate Bersch,*[,||] Bernhard Brutscher,[||] Martin Blackledge,[||] and Jacques Covès*[,‡]

Laboratoire de Chimie et Biochimie des Centres Rédox Biologiques, CEA-Grenoble, DBMS/CB, UMR 5047 CNRS-CEA-UJF, 17, Avenue des Martyrs, 38054 Grenoble Cedex 9, France, and Laboratoire de Résonance Magnétique Nucléaire, Institut de Biologie Structurale−Jean-Pierre Ebel, UMR 5075 CNRS-CEA-UJF, 41, rue Jules Horowitz, 38027 Grenoble Cedex 1, France

Received December 5, 2001; Revised Manuscript Received January 15, 2002

ABSTRACT: The flavodoxin-like domain, missing in the three-dimensional structure of the monomeric, simplified model of the *Escherichia coli* sulfite reductase flavoprotein component (SiR-FP), has now been expressed independently. This 168 amino acid protein was named SiR-FP18 with respect to its native molecular weight and represents the FMN-binding domain of SiR-FP. This simplified biological object has kept the main characteristics of its counterpart in the native protein. It could incorporate FMN exclusively and stabilize a neutral air-stable semiquinone radical. Both the radical and the fully reduced forms of SiR-FP18 were able to transfer their electrons to DCPIP or cytochrome *c* quantitatively. SiR-FP18 was able to form a highly stable complex with SiR-HP, the hemoprotein component of the sulfite reductase containing an iron−sulfur cluster coupled to a siroheme. In agreement with the postulated catalytic cycle of SiR-FP, only the fully reduced form of SiR-FP18 could transfer one electron to SiR-HP, the transferred electron being localized exclusively on the heme. As isolated SiR-FP18 has kept the main characteristics of the FMN-binding domain of the native protein, a structural analysis by NMR was performed in order to complete the partial structure obtained previously. Structural modeling was performed using sequence homologues, cytochrome P450 reductase (CPR; 29% identity) and bacterial cytochrome P450 (P450-BM3; 26% identity), as conformational templates. These sequences were anchored using common secondary structural elements identified from heteronuclear NMR data measured on the protein backbone. The resulting structural model was validated, and subsequently refined using residual ($C^{\alpha}-C'$, $N-H^N$, and $C'-H^N$) dipolar couplings measured in an anisotropic medium. The overall fold of SiR-FP18 is very similar to that of bacterial flavodoxins and of the flavodoxin-like domain in CPR or P450-BM3.

Sulfite reductase (SiR)[1] from *Escherichia coli* is a multimeric and soluble hemoflavoprotein that mediates the transfer of electrons from NADPH to sulfite to produce sulfide. This reaction is a key step of the sulfate assimilation pathway leading to the biosynthesis of organic sulfur compounds such as L-cysteine (*1*). SiR was originally described as an $\alpha_8\beta_4$ polymer (*2*). The homooctameric α_8 complex is the flavoprotein component (SiR-FP) of the enzyme as each α-chain binds one FAD and one FMN and, in addition, contains an NADPH-binding domain (*3*, *4*). The module constituted of the FAD- and NADPH-binding domains is homologous to the ferredoxin−$NADP^+$ reductases whereas the FMN-binding domain is homologous to bacterial flavodoxins. This kind of organization is characteristic of the family of proteins that includes NADPH−cytochrome P450 reductase (CPR), nitric oxide synthase, and *Bacillus megaterium* cytochrome P450 (P450-BM3) (*5*−*7*). The role of SiR-FP is to transfer electrons from NADPH via the FAD and the FMN prosthetic groups to the β-subunit (*8*). SiR-FP is also able to transfer electrons either from the FMN site to artificial acceptors such as ferricyanide, dichlorophenol indophenol, or cytochrome *c*, while FAD can reduce directly $AcPyADP^+$ or free exogenous flavins (*3*, *8*, *9*). Each β-protein contains an Fe_4S_4 cluster coupled to a siroheme through a cysteine bridge and corresponds to the hemoprotein component (SiR-HP) of the protein. The siroheme finally transfers the electrons to sulfite for its reduction to sulfide (*8*, *10*).

The crystal structure of SiR-HP has already been determined (*10*). However, native or recombinant SiR holoenzyme has so far resisted crystallization. Therefore, we have developed a molecular dissection strategy of the SiR molecule in order to create new simplified biological objects corresponding to the different functional modules of the protein

† This work was supported by the Centre National de la Recherche Scientifique (CNRS) and the Commissariat à l'Energie Atomique (CEA).

* To whom correspondence should be addressed. J.C.: Telephone 33-(0)4-38-78-91-22, FAX 33-(0)4-38-78-91-24, E-mail jcoves@cea.fr. B. Bersch: Telephone 33-(0)4-38-78-48-25, FAX 33-(0)4-38-78-54-94, E-mail beate.bersch@ibs.fr.

‡ Laboratoire de Chimie et Biochimie des Centres Rédox Biologiques, CEA-Grenoble.

§ These authors have equally contributed to this work.

|| Laboratoire de Résonance Magnétique Nucléaire, Institut de Biologie Structurale−Jean-Pierre Ebel.

[1] Abbreviations: CPR, cytochrome P450 reductase; CSI, chemical shift index; DCPIP, dichlorophenol indophenol; FAD, flavin adenine dinucleotide; FMN, flavin mononucleotide; HSQC, ^{1}H-detected heteronuclear single quantum coherence; NOE, nuclear Overhauser effect; P450-BM3, *Bacillus megaterium* cytochrome P450; RDC's, residual dipolar couplings; SiR, sulfite reductase; SiR-FP, sulfite reductase flavoprotein component; SiR-HP, sulfite reductase hemoprotein component.

10.1021/bi016008i CCC: $22.00
Published on Web 02/13/2002

[for a review, see (*11*)]. Among them, a monomeric simplified model of SiR-FP was constructed by deletion of the first 51 N-terminal amino acids of the α-polypeptide, thus removing the determinants required for octamerization (*12*). The truncated protein, previously called SiR-FP60, was demonstrated to be a monomer with FAD and FMN as cofactors and displaying all the catalytic diaphorase activities of SiR-FP. Moreover, we have demonstrated that incubation of SiR-FP60 with SiR-HP led to a stable and functional $\alpha_1\beta_1$ complex able to oxidize NADPH at the expense of sulfite (*13*).

The crystal structure of SiR-FP60 has been determined at 1.94 Å resolution (*14*). Unfortunately, in the four different crystal forms obtained, the FMN-binding domain was absent from the electron density although its presence was demonstrated within the crystal. This was interpreted as a flexibility of the flavodoxin-like domain required for optimal electron transfer. To complete the crystal structure, we report the expression of a monomeric version of the flavodoxin-like domain of SiR-FP. This new protein was named SiR-FP18 with respect to its native molecular weight. We describe here the specific characterization of SiR-FP18 and its comparison with SiR-FP23, the polymeric FMN-binding domain of SiR-FP (*15*). The overall chemical reactivity of this protein makes it a very good model of its polymeric counterpart. These results are complemented by structural information obtained on SiR-FP18. Using multidimensional NMR, the secondary structure and the topology of SiR-FP18 have been determined. A structural model was built using sequence similarity and then validated and refined using heteronuclear residual dipolar couplings (RDC's) measured in an anisotropic medium. It is demonstrated that, using RDC's, an experimentally verified low-resolution structural model can be obtained rapidly after assignment of the backbone resonances. As expected, SiR-FP18 shows very close structural homology with the corresponding modules in CPR and P450-BM3 whose three-dimensional structures have been determined by X-ray crystallography (*16*−*18*).

EXPERIMENTAL PROCEDURES

Construction of the Expression Plasmid, and Expression and Purification of the Recombinant SiR-FP18 Protein. The DNA fragment expected to encode for the monomeric form of the flavodoxin-like domain of SiR-FP was amplified by PCR with suitable restriction sites for subcloning in the expression vector pET30. The sense primer 5′-ACGGAATTCATATG**GCAACGCCAGCGCCAGCTGCAGAAATGC** contains the nucleotides (in boldface type) coding for an N-terminal amino acid sequence starting with alanine-52 (ATPAPAAEM). The overhanging sequence includes an *Nde*I site (underlined) carrying the initiator codon ATG. The antisense primer 5′-GGCGGATCCTCA**AGCGACGGATTGCGAAGGTGC** was designed to incorporate a *Bam*HI site (underlined) and a stop codon in the coding sequence of SiR-FP to construct a protein truncated between alanine-219 and threonine-220. The nucleotides (in boldface) are complementary of the corresponding coding sequence of SiR-FP. The authenticity of the DNA insert generated by PCR was confirmed by sequencing. The resulting expression plasmid pET-SiR-FP18 was used to transform the T7 RNA polymerase-containing host *E. coli* BL21(DE3). The freshly transformed bacteria were grown at 37 °C in M9 minimal mineral medium with glucose (2 g/L) as carbon source and supplemented with $MnCl_2$ (0.1 mM), $ZnSO_4$ (0.05 mM), $FeCl_3$ (0.05 mM), and a vitamin solution according to Jansson et al. (*19*). Isotopically labeled protein was prepared by growing the cells with $^{15}NH_4Cl$ (1 g/L) and $^{13}C_6$-glucose (2 g/L) as sole nitrogen and carbon sources. A triply labeled sample ($^2H/^{15}N/^{13}C$) was obtained in the same medium prepared with 90% ^2H_2O. Protein expression was induced by the addition of 0.5 mM isopropyl-1-thio-β-D-galactopyranoside when cells reached an A_{600} between 0.5 and 0.6. Cells were harvested by centrifugation after 4 h of incubation at 37 °C. In the specific case of the triply labeled sample, incubation after induction was for 8 h at 37 °C.

The pellet from 1 L of culture was suspended in 100 mM Tris/HCl (pH 7.5) and lysed by sonic oscillation. The total protein extract was recovered by centrifugation for 90 min at 45 000 rpm in a 50.2 TI rotor (Beckman) and used for further purification. The total protein extract (100 mg of protein) was treated as previously described for the purification of SiR-FP (*3*). The pellet obtained after ammonium sulfate precipitation (80% final saturation) was dissolved in a minimal volume of 100 mM potassium phosphate buffer (pH 7.0). Potassium ferricyanide was added at a final concentration of 1 mM before the protein solution was subjected to filtration on a Superdex-75 column (Amersham-Pharmacia Biotech) previously equilibrated with the same buffer. Elution was run at 0.8 mL·min^{-1}, and 1 mL fractions were collected. Fractions were assayed for protein (absorbance at 280 nm) and for flavin content (absorbance at 450 nm). Flavin-containing fractions were pooled and concentrated by ultrafiltration using a Diaflo cell equipped with a YM-10 membrane (Amicon Co.) and Centricon-10 microconcentrators. At this stage, SiR-FP18 was electrophoretically pure. The yield for a typical purification procedure is 30−35 mg of pure SiR-FP18 from 1 L of minimal medium.

Protein concentration was determined using bovine serum albumin as a standard (*20*) and the commercial Bio-Rad protein assay solution. The denatured molecular mass of SiR-FP18 was estimated by 0.1% SDS−15% polyacrylamide gel electrophoresis (*21*), and its native molecular mass was ascertained by elution of a calibrated Superdex-75 filtration column.

Cofactor Analysis and Reconstitution of SiR-FP18. A sample of pure SiR-FP18 was boiled for 10 min in the dark, chilled on ice, and microcentrifuged for 10 min to pellet the denatured protein. An aliquot of the supernatant was analyzed by thin-layer chromatography on silica gel 60 F_{254} (Merck) and developed with butan-1-ol/acetic acid/water (12:3:5, by volume). Pure FMN and FAD were run separately or as a mixture under the same conditions as a control.

For reconstitution experiments, SiR-FP18 was incubated with a 2-fold excess of either FMN, FAD, or riboflavin for 60 min at ice temperature in the dark. Excess flavin was removed in a first step by filtration on Sephadex G-25. Nonspecifically bound flavin was then removed by two cycles of dilution in 50 mM Tris/HCl, pH 7.5, containing 250 mM NaCl, followed by concentration on Centricon-10. Optical spectra of SiR-FP18 were recorded before and after reconstitution. In each case, the concentration of protein-bound flavin was calculated after heat-denaturation of the protein from the absorbance of the free cofactor. An extinction coefficient of 12.2 mM^{-1}·cm^{-1} at 450 nm was

used for FMN and riboflavin, and 11.3 $mM^{-1}\cdot cm^{-1}$ for FAD at the same wavelength (*22*).

For NMR experiments, SiR-FP18 in potassium phosphate buffer was reconstituted by dilution with a slight excess of pure commercial FMN (Sigma). The protein sample was then concentrated on Centricon-10, washed once with the same buffer to remove the excess of FMN, and transferred to the NMR tube for further use.

Reduction of SiR-FP18 and Reactivity of the Reduced Protein. For the titration experiments, the protein sample was made oxygen-free by overnight incubation in a glovebox under overpressure of nitrogen. Sodium dithionite solutions were prepared in anaerobic buffers. Dithionite concentration was calculated using an extinction coefficient of 8 $mM^{-1}\cdot cm^{-1}$ at 315 nm. At the end of the experiments, the stability of the titrant was checked using the same method. After each addition of titrant, the solution was left for at least 10 min at room temperature to reach the thermodynamic equilibrium before recording a spectrum. Protein conditions are detailed under Results or in the legend of the corresponding figures.

Photochemical reductions in the presence of deazaflavin−EDTA were carried out as previously described (*15*). The one-electron-reduced form of SiR-FP18 ($FMNH^{\bullet}$) was generated by oxidation of the fully reduced form upon air admission.

The chemical reactivity of the two-electron-reduced form ($FMNH_2$) or of the one-electron-reduced form ($FMNH^{\bullet}$) of SiR-FP18 was assayed as outlined previously for SiR-FP23 with cytochrome *c* as an electron acceptor (*15*). DCPIP was also used in place of cytochrome *c*. In this case, the absorbance change was followed at 600 nm using an absorption coefficient of 21 $mM^{-1}\cdot cm^{-1}$.

In the same way, SiR-HP, the hemoprotein component of the sulfite reductase, was used as an electron acceptor from the reduced forms of SiR-FP18. The one-electron-reduced form obtained by air oxidation of the fully reduced form was deaerated by prolonged incubation in the glovebox before its reactivity was checked under anaerobiosis. The absorbance changes upon electron transfer were followed spectrophotometrically by recording the absorption spectra of the mixture of a slight molar excess of SiR-FP18 with respect to SiR-HP. Once the reaction finished, the mixture was transferred to an EPR tube. The tubes were frozen under anaerobiosis, capped with a rubber septum, and analyzed by EPR spectroscopy as described below and in the legends of the corresponding figures. Then, the content of two tubes was thawed under anaerobiosis, and each solution was mixed with an excess of sulfite (500 μM) before being analyzed again by EPR spectroscopy.

Alternatively, visual observation of the oxidation of the reduced forms of SiR-FP18 was performed with potassium ferricyanide as an oxidant.

Affinity Chromatography. The capacity of SiR-FP18 and SiR-HP to form a stable complex was checked by affinity chromatography. SiR-FP18 was coupled to CNBr-activated Sepharose 4B (Amersham-Pharmacia Biotech) as described by the manufacturer. The gel was then incubated overnight under constant agitation at room temperature with an excess of SiR-HP. A column of 200 μL was packed, and unbound SiR-HP was removed by washing the gel with 3 volumes of 50 mM Tris/HCl, pH 7.5 (buffer A). The column was then washed with 3 volumes of buffer A containing 0.5 M NaCl and then with 3 volumes of buffer A containing 1 M NaCl. The time of contact of the gel with these high ionic strength solutions was at least 15 min. Finally the gel was incubated overnight in the presence of 5 M urea before being washed again with buffer A. The beads were then removed from the column, and the suspension was boiled in electrophoresis denaturing buffer for 10 min.

Spectroscopic Methods. UV−visible spectra of aerobic samples were recorded at 25 °C in a quartz cell (10 mm light path) using a Cary 1 Bio (Varian) or a Uvikon 930 (Kontron) spectrophotometer. For recording the absorption spectra of anaerobic samples, a cuvette holder inside a glovebox under overpressure of nitrogen was connected with optical fibers to a Hewlett-Packard 8452A diode array spectrophotometer.

EPR spectra were recorded with a Bruker EMX spectrometer operating at 9.45 GHz and equipped with an ESR 900 helium flow cryostat (Oxford Instruments). Neutral semiquinone radical on flavin was quantified by comparison with a sample of SiR-FP60 containing a known amount of FMN radical (*12*).

All NMR experiments were performed on Varian INOVA 600 and INOVA 800 spectrometers, both equipped with a triple-resonance (^1H, ^{15}N, ^{13}C) probe and shielded z-gradients. The FMN-reconstituted oxidized protein was dissolved to a final concentration of about 1.2 mM in 90% H_2O, 10% D_2O containing 100 mM sodium phosphate, pH 7.0, and 0.02% sodium azide. The sample temperature was set to 30 °C. Quadrature detection in the indirect dimensions of the multidimensional experiments was achieved by the echo/antiecho detection scheme for ^{15}N, and by the TPPI-States method for ^1H. A three-dimensional ^{15}N-edited NOESY spectrum was obtained at 800 MHz with the NOESY mixing time set to 100 ms. Eight scans were recorded per (t_1, t_2) increment. For the deuterium exchange, the protein was lyophilized in a SpeedVac (Savant) and suspended in D_2O buffer. ^1H, ^{15}N HSQC spectra were acquired after 15 min, 12 h, and 1 month to identify the slowly exchanging amide protons.

Hydrogen bonds were established according to Cordier and Grzesiek (*23*) by the detection of cross-hydrogen bond $^{15}N-^{13}C'$ scalar couplings ($^{3h}J_{NC'}$) in a long-range HNCO experiment at 800 MHz. Residual dipolar couplings (RDC's) were collected on a 1.6 mM uniformly ^{13}C, ^{15}N- and 70% ^2H-labeled sample suspended in a liquid-crystalline medium consisting of a 14 mg/mL aliquot of the filamentous phage Pf1 (Asla Ltd, Riga, Latvia) in 100 mM potassium phosphate buffer, pH 7.0, containing 2 mM $MgCl_2$. Three different types of dipolar couplings were measured at 600 MHz: $^1D_{NH}$, $^1D_{C'C\alpha}$, and $^2D_{C'HN}$ couplings were obtained using 3D HNCO-type experiments (*24*, *25*).

Data processing and peak picking were performed using FELIX program version 2000 (Accelrys Inc.).

Homology Modeling. A structural model for SiR-FP18 was built by homology modeling using SWISS-MODEL and the Swiss-PdbViewer (*26*). The crystal structures of the flavodoxin-like domains of human CPR [pdb code 1B1C, (*17*)] and P450-BM3 [pdb code 1BVY, (*18*)] were used as templates. For the initial project file, a structural alignment was built using the Swiss-PdbViewer considering protein sequence similarity and identification of secondary structure elements. Secondary structure information was derived from

the analysis of the deviation of the experimental ^{13}C chemical shifts from random-coil values [chemical shift index, CSI, (*27*)], the intensity distribution of short- and medium-range NOEs involving H^N protons, and the presence of hydrogen bonds. This alignment was then submitted to SWISS-MODEL for final modeling.

Model Validation Using Module. The homology-based model, corresponding to residues 60−210 of SiR-FP, was further validated by using long-range structural information obtained from RDC data. The recently developed program Module (*28*) was used to evaluate the accordance between the structural model calculated with SWISS-MODEL and the experimental RDC data. Module determines alignment tensor parameters and provides a graphical interface for the visualization of the tensor relative to the three-dimensional atomic coordinates as well as correlation plots of the measured and calculated couplings. In the initial stage, the secondary structure elements were treated as separate structural entities. The alignment tensor is characterized by five parameters: the axial and rhombic components, A_a and A_r, measure the extent of residual alignment due to the restricted orientational sampling in the anisotropic medium, whereas the Euler angles, $\{\alpha, \beta, \gamma\}$, define the nonaveraged orientation of the molecule in the three-dimensional space. For each entity, these five parameters were determined using nonlinear least-squares minimization of the target function over all couplings associated with a given domain:

$$\chi^2 = \sum_n \{D_{ij}^{exp} - D_{ij}^{calc}\}^2/\sigma_{ij}^2 \quad (1)$$

where D_{ij} are the residual dipolar couplings between spins i and j and σ_{ij} is the uncertainty in the experimentally measured coupling. σ_{ij} was set to 1 Hz for all couplings.

The quality of the model structure can be evaluated by comparing measured dipolar couplings with dipolar couplings back-calculated from the best-fit alignment tensor. Additional information can be obtained from comparison of the amplitude and orientation of the individual alignment tensors for the different structural elements. In the case of a rigid molecule, A_a and A_r should be identical for each structural entity. Differences would indicate differential flexibility. On the other hand, the orientation of the individual alignment tensors should be coaxial, if the relative orientation of the secondary structure elements in the model structure is correct.

Refinement Using Sculptor. The initial structural model was further refined with the program Sculptor (*29, 30*), using a restrained molecular dynamics protocol, incorporating residual dipolar couplings as experimental restraints.

The homology-based model was initially fixed, and the alignment tensor was optimized using an energy minimization protocol under the influence of residual dipolar couplings from the secondary structural elements. This alignment tensor is then identical to the tensor determined using the program Module. Following this, the molecule was released and allowed to evolve under the influence of RDC's, backbone dihedral angle restraints in the secondary structural elements, measured NOE's from the β-sheet motif, and hydrogen bonds identified from the direct measurement via scalar coupling. As RDC's contain only orientational information and no translational restriction, a tethering potential was applied on the C_α atoms of the peptide chain in order to avoid simple expansion of the molecular model. This energy term is applied as a sum over all C_α atoms; global unfolding is thus avoided while allowing local reorientation. A potential of the form

$$E_{teth} = k_{teth}\sum_i \sqrt{(x_i - x_i^0)^2/N} \quad (2)$$

was incorporated into the potential energy function. x_i are the Cartesian coordinates of the atoms to be tethered and x_i^0 the target coordinates. The force constant k_{teth} (20 kcal·mol^{-1}·Å^{-2}) is used to restrain the $N = 156$ atoms to the coordinates of the initial model structure.

The system was then equilibrated at 300 K for 0.5 ps of molecular dynamics, and gradually increased to 500 K over a period of 2 ps, during which time $k_{NOE,H\text{-}bond}$, k_{dihe}, and k_{RDC} were raised from their initial (0.1, 0.1, 0.001) to their final values (50.0 kcal·mol^{-1}·Å^{-2}, 100.0 kcal·mol^{-1}·deg^{-2}, $k_{RDC,i,j}$). The energetic weighting of the different types of RDC was initially estimated on the basis of the precision of the different experimental measurements ($\sigma_{ij} = 1.0$ Hz for ^{N}H−N, C_α−C′, and ^{N}H−C′) and then empirically adjusted such that the final structures had a total reduced χ^2 (χ^2/N where N is the number of couplings) close to 1. Final force constants of $k_{RDC,N-H} = 0.63$ kcal·mol^{-1}·Hz^{-2}, $k_{RDC,C\alpha-C'} = 1.11$ kcal·mol^{-1}·Hz^{-2}, and $k_{RDC,NH-C'} = 1.11$ kcal·mol^{-1}·Hz^{-2} were used.

During the sampling period, the molecule and tensors evolved freely for 2 ps before the system was cooled to 100 K over 7 ps and the system minimized using a conjugate gradient algorithm. A total of 30 calculations were performed using different initial atomic velocity distributions; the 10 structures with the lowest total target function comprising NOE, backbone torsion, hydrogen bonding, and RDC restraints were selected for final analysis. This set of calculations was repeated using no RDC data, to test for force-field, or protocol-dependent effects, and serves as a control for the calculations that included the RDC's.

RESULTS

Overexpression, Purification, and Characterization of SiR-FP18. E. coli BL21(DE3) was transformed with the expression plasmid pET-SiR-FP18 encoding SiR-FP18, a protein corresponding to the FMN-binding domain of SiR-FP but with alanine-52 as the first residue and alanine-219 as the last one. Maximal expression was observed between 4 and 8 h after addition of IPTG to the cell cultures depending on the characteristics of the growth medium (4 h in H_2O and 8 h in ^2H_2O). SiR-FP18 was recovered in the soluble extracts which were blue−gray. Their UV−visible spectrum was dominated by a long-wavelength absorption band at 589 nm and a shoulder at 630 nm characteristic of the presence of FMNH$^\bullet$. This indicated the large accumulation of a flavoprotein under the blue neutral semiquinone state as previously observed for SiR-FP23 (*15*) and SiR-FP60 (*12*). SDS−PAGE analysis of the crude extracts showed a predominant band at an apparent molecular mass of 18 kDa corresponding to the expected mass of SiR-FP18 (not shown). The overproduced protein was then purified to homogeneity by a one-step procedure. The ammonium sulfate pellet was resuspended in a minimal volume of potassium phosphate buffer,

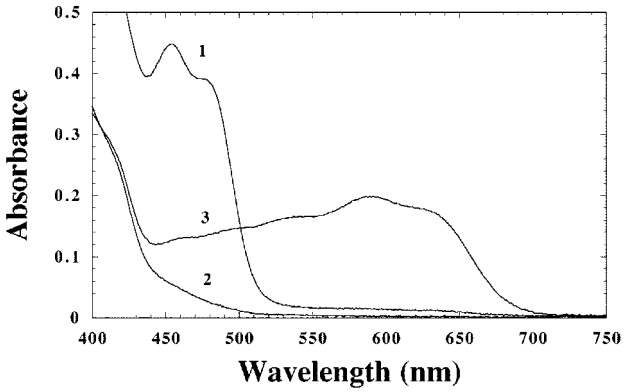

FIGURE 1: Absorption spectra of the three redox states of SiR-FP18. Spectrum 1, oxidized SiR-FP18 (40 μM in FMN); spectrum 2, fully reduced state obtained by anaerobic photoreduction in the presence of deazaflavin−EDTA as described under Experimental Procedures; spectrum 3, air-stable semiquinone state obtained from a short incubation of fully reduced SiR-FP18 with air. Note that the contribution of the oxidized deazaflavin−EDTA system is visible below 430 nm in spectrum 1.

and 1 mM ferricyanide was added in order to oxidize the protein. The solution turned instantaneously yellow under these conditions and was fractionated on a Superdex-75 filtration column. Flavin-containing fractions corresponding to a native molecular mass of about 20 kDa were pooled. SDS−PAGE analysis of these fractions revealed the presence of an 18 kDa protein corresponding to the overproduced protein contained in the extracts. This showed that SiR-FP18 is a monomer as expected. A yield of about 30 mg of pure protein per liter of culture was routinely obtained. Isotopically labeled protein was produced for NMR experiments. The extent of isotopic labeling was checked by electrospray ionization mass spectroscopy analyses by comparison of the molecular mass of pure unlabeled SiR-FP18 with that of the labeled proteins. The extent of labeling was >97% for ^{15}N and ^{13}C and 70% for ^{2}H. Analysis of the flavin cofactor in pure SiR-FP18 was done by thin-layer chromatography of the supernatant of a heat-denaturated protein sample. This confirmed that, as expected, SiR-FP18 contained FMN exclusively. Quantification of the FMN content was performed by spectrophotometric analysis of the same supernatant using an extinction coefficient of 12.2 $mM^{-1}\cdot cm^{-1}$ at 450 nm. We calculated a ratio of 0.25−0.6 mol of FMN per mole of SiR-FP18 depending on the protein preparation. This shows that, as previously observed for SiR-FP23 (*15*), SiR-FP18 can be largely depleted of its flavin cofactor, likely due to the large overexpression of the protein. An extinction coefficient of 11.3 $mM^{-1}\cdot cm^{-1}$ at 456 nm (the absorption maximum) was estimated in the fully oxidized state. As for SiR-FP23, the visible spectrum of SiR-FP18 also presents a characteristic shoulder at 480−490 nm (Figure 1, spectrum 1).

Incubation of SiR-FP18 with an excess of FMN led to a reconstituted protein containing 1 mol of FMN per mole of protein. As previously observed with SiR-FP23, reconstitution of SiR-FP18 with riboflavin or FAD was shown to be ineffective. This indicates that SiR-FP18 presents the correct fold allowing for the exclusive binding of FMN.

Reduction of SiR-FP18 and Reactivity of the Reduced Protein. Photoreduction of fully oxidized SiR-FP18 (85 μM total flavin concentration) was achieved by illumination at pH 7.5 and under anaerobic conditions in the presence of 20 μM deazaflavin and 10 mM EDTA. The reduction proceeds in two distinct steps (not shown) exactly as observed with SiR-FP23 (*15*). During the first step, the absorbance at 456 nm decreased while a long-wavelength absorption band at 589 nm with a shoulder at 630 nm, characteristic of the neutral blue semiquinone previously observed in the total extracts, increased in parallel. These spectral changes occurred with the isosbestic point at 504 nm, which was demonstrated to be characteristic of the transition from the oxidized form of the protein to its one-electron-reduced form (*12*, *15*). The second step was characterized by the concomitant decrease of both bands at 456 and 589 nm until the protein was reduced to the hydroquinone state (Figure 1, spectrum 3). Upon air admission, the fully reduced form was converted almost instantaneously to the air-stable radical form (Figure 1, spectrum 2). This stability allows an accurate quantification of the spin concentration by EPR spectroscopy. The X-band EPR spectrum of the flavin semiquinone radical was recorded at 20.5 K and then compared to that of a solution of SiR-FP60 containing a known amount of $FMNH^{\bullet}$ (*12*). The experiment was run with SiR-FP18 obtained after purification and thus partially depleted in FMN as well as with a fully reconstituted protein. Starting with a preparation of SiR-FP18 containing 300 μM FMN in the first case and 100 μM in the second case, 290 and 92 μM radical were obtained, respectively, for the partially depleted and the reconstituted protein. We can thus conclude that respectively 96% and 92% of the $FMNH_2$ was converted to the semiquinone form. An average value of the extinction coefficient at 589 nm of 4.5 $mM^{-1}\cdot cm^{-1}$ was estimated from these results. This value is situated between the value of 4.88 $mM^{-1}\cdot cm^{-1}$ obtained with SiR-FP23 and of 4 $mM^{-1}\cdot cm^{-1}$ obtained with SiR-FP (*9*).

The spectral changes associated with dithionite titration of SiR-FP18 were also recorded spectrophotometrically under anaerobic conditions (not shown). As expected, addition of 1 electron-equiv (0.5 mol of dithionite per mole of protein-bound FMN) resulted in spectral changes characteristic of the formation of $FMNH^{\bullet}$. We could calculate that about 100% $FMNH^{\bullet}$ was generated under these conditions. After a second electron-equivalent was added, a spectrum characteristic of the hydroquinone form of SiR-FP18 was obtained.

The ability of the reduced forms of SiR-FP18 to transfer electrons to dichlorophenol indophenol has been assayed. Fully photoreduced or semi-reduced SiR-FP18, containing 10 μM $FMNH_2$ or 10 μM $FMNH^{\bullet}$, respectively, was mixed with an excess of oxidized DCPIP (30 μM). The spectral changes due to DCPIP reduction were recorded spectrophotometrically. Using an extinction coefficient of 21 $mM^{-1}\cdot cm^{-1}$ at 600 nm for DCPIP, it was easy to calculate that respectively 21 or 10 μM DCPIP was reduced almost instantaneously. This shows that the two reduced forms of SiR-FP18 can transfer quantitatively their electrons to such an acceptor. It should be noted that, as neither the protein nor the dye has a significant absorbance at 600 nm when oxidized, no spectrum correction is required as is the case when the same experiment is run with cytochrome *c*. Indeed, the same quantitative and immediate electron transfer was also observed with cytochrome *c* as an oxidant. Ferricyanide was also used qualitatively to oxidize the protein present

under the semiquinone state in the soluble extracts before purification.

Finally, fully or one-electron-reduced SiR-FP18 (100 μM) was also mixed under anaerobiosis with oxidized SiR-HP (80 μM), the physiological partner of SiR-FP in native sulfite reductase. The reaction between the two proteins was followed spectrophotometrically. In both cases, the resulting experimental spectra resembled the calculated spectrum resulting from the addition of SiR-HP plus one-electron-reduced SiR-FP18. In addition, subtraction of the SiR-HP spectrum from the experimental ones resulted in spectra characteristic of the semiquinone species (not shown). This suggests that only the fully reduced SiR-FP18 had transferred one electron to SiR-HP and that the one-electron-reduced form of SiR-FP18 was not reactive with oxidized SiR-HP. To validate this hypothesis, the EPR spectra of the two different mixtures were recorded at helium temperature (Figure 2). In both cases (Figure 2A,B), the presence of the organic radical characteristic of the flavin semiquinone was evident at $g = 2$. Quantification of these signals at 30 K gave a value of about 92 μM FMN under the semireduced state. The EPR spectrum of the solution resulting from the mixture SiR-HP plus one-electron-reduced SiR-FP18 contained in addition the signal characteristic of a high-spin $S = 5/2$ ferrisiroheme with the features at $g = 6.65$ and 5.23 clearly visible (Figure 2A). This signal was almost absent after reaction of SiR-HP with fully reduced SiR-FP18 (Figure 2B), demonstrating that the majority of the ferrisiroheme was converted to ferrosiroheme (probably to the low-spin state $S = 0$). The spectrum of a $S = 1/2$ $(Fe_4S_4)^+$ cluster was absent, showing that SiR-HP was only reduced by one electron with this electron localized on the heme. This electron originates from the hydroquinone form of SiR-FP18 which was converted in turn to the semiquinone form. Moreover, after addition of sulfite, the remaining signal of the ferrisiroheme disappeared completely (Figure 2C). This experiment demonstrates clearly that (i) SiR-HP and SiR-FP18 do interact, (ii) electron transfer is possible between these two proteins, and (iii) only the hydroquinone form can give one electron to SiR-HP.

SiR-FP18 and SiR-HP Form a Stable Complex. SiR-HP was incubated with SiR-FP18 previously coupled to CNBr-activated Sepharose 4B and packed to a small column. The column was first washed with a standard buffer in order to remove unbound SiR-HP (Figure 3, lane 1). Then, the column was extensively washed with the same buffer containing 0.5 M NaCl (Figure 3, lane 2) and 1 M NaCl (Figure 3, lane 3). The use of a chaotropic agent (5 M urea) was also inefficient in eluting bound SiR-HP (Figure 3, lane 4). SiR-HP could be recovered only after incubation of the gel beads with denaturing electrophoresis buffer (Figure 3, lane 5). This demonstrates unambiguously the very tight association of the two proteins under these conditions. The same experiment was repeated with BSA in place of SiR-HP as a control, and no binding of BSA on SiR-FP18 was observed (not shown).

Secondary Structure and Global Fold. The complete NMR backbone and side-chain assignment of SiR-FP18 has been previously reported (*31*). Secondary structure information was derived from the analysis of different NMR parameters. These results are summarized in Figure 4A. SiR-FP18 is composed of five β-strands (residues 63−69, 92−95, 110−116, 146−151, and 183−186) and four α-helices (residues 72−87, 128−133, 163−173, and 190−205). A small, additional β-strand named 5a (residues 177−179) can also be proposed based on the observation of hydrogen bonds and sequential NOEs and in analogy to the flavodoxin-like

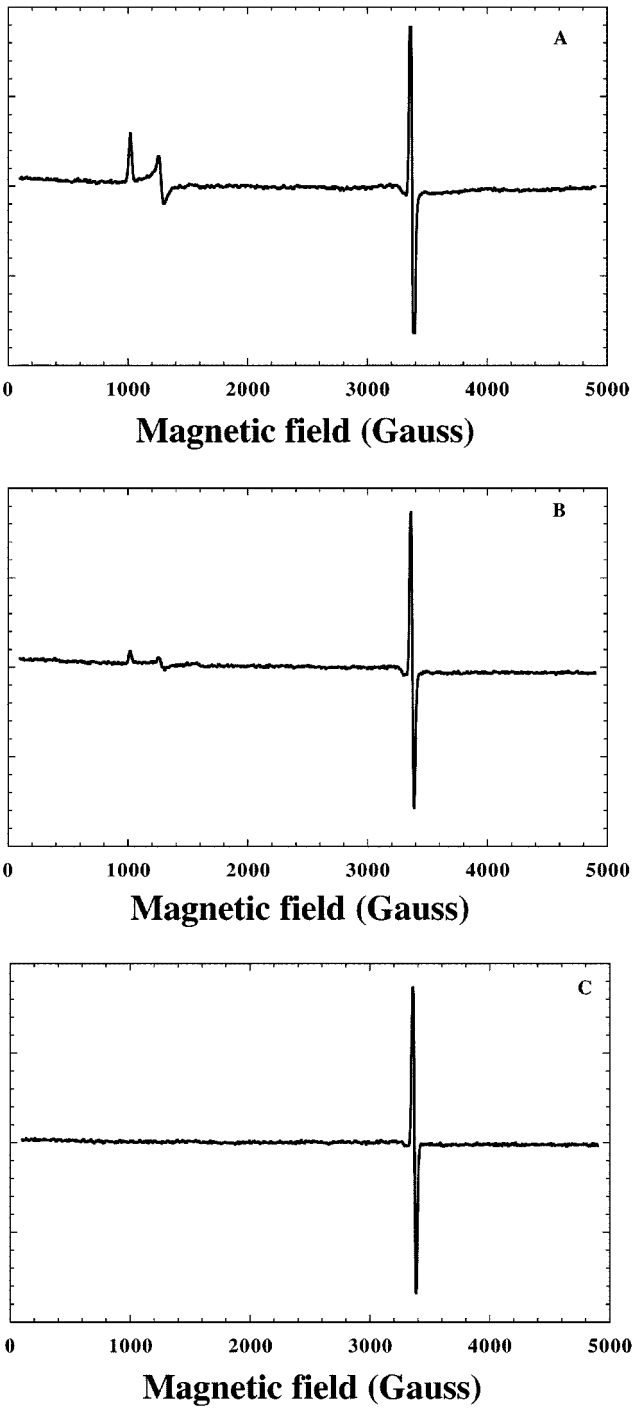

FIGURE 2: EPR characterization of the reaction between reduced SiR-FP18 and SiR-HP. The concentrations of SiR-FP18 and SiR-HP were respectively 100 μM in FMN and 80 μM in the three experiments. (A) X-band EPR spectrum obtained after anaerobic incubation of semireduced SiR-FP18 with SiR-HP. (B) X-band EPR spectrum obtained after anaerobic incubation of fully reduced SiR-FP18 with SiR-HP. (C) 500 μM sodium sulfite was added to the previous solution before recording the X-band EPR spectrum. EPR conditions were as follows: temperature, 9 K; modulation amplitude, 1 mT; microwave power, 1 mW; microwave frequency, 9.449, 9.448, or 9.443 for spectra A−C.

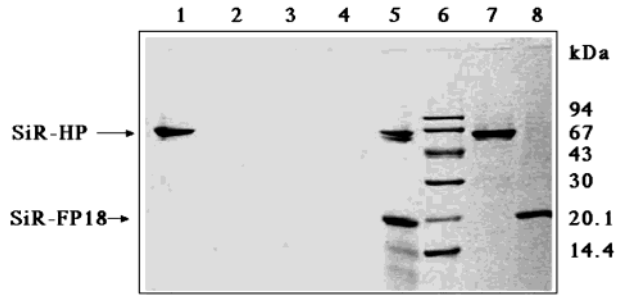

FIGURE 3: SiR-FP18 and SiR-HP form a tight complex. SiR-HP has been incubated with SiR-FP18 previously coupled to CNBr-activated Sepharose-4B as described under Experimental Procedures. The fractions issued from the elution procedure were analyzed by SDS−PAGE. Lane 1, unbound SiR-HP eluted with 50 mM Tris/HCl, pH 7.5 (buffer A); lanes 2−4, fractions eluted with buffer A containing in addition 0.5 M NaCl or 1 M NaCl or 5 M urea, respectively; lane 5, proteins obtained after incubation of the gel beads in the electrophoresis denaturing buffer; lane 6, low molecular weight markers; lanes 7 and 8, pure SiR-HP and SiR-FP18, respectively, run as a control.

domain of CPR (*17*). Hydrogen bonds were initially detected by slow exchange rates of the amide protons acting as hydrogen bond donors. To complete this information, cross hydrogen bond scalar couplings were measured to directly correlate hydrogen bond donors to the corresponding acceptors. The complete hydrogen bond networks stabilizing the α-helices as well as those connecting the individual β-sheets have thus been detected. In combination with long-range H^N-H^α NOE, these data allowed the determination of the topology of the central β-sheet (Figure 4B). The strands form a parallel β-sheet with strands ordered as follows: 2, 1, 3, 4, 5. The distribution of the slowly exchanging amide protons indicates that β-strands 2 and 5 are partially solvent-exposed (see Figure 4A,B). These observations show that the topology of the central β-sheet is close to the bacterial flavodoxins and the flavodoxin-like domains of CPR and P450-BM3. The NMR spectra obtained with a largely FMN-depleted sample of SiR-FP18 were very similar to those obtained with a fully reconstituted protein (not shown). This indicates that folding of SiR-FP18 is not dependent on the presence of the FMN cofactor.

To obtain a more detailed structural model of SiR-FP18, we have undertaken homology modeling followed by a validation and refinement process based on experimental long-range structural information obtained from RDC data. The model structure (residues 60−210) obtained from SWISS-MODEL is very close to the two template structures (heavy atom rmsd calculated over the secondary structure elements of 0.52 and 0.71 Å for the corresponding domains in human CPR and P450-BM3, respectively).

This model structure was then compared to the experimental RDC data. Three sets of residual dipolar couplings defining the backbone conformation of the peptide chain were used as input data in the program Module (*28*). Individual analyses were performed using RDC's from the five different secondary structural elements identified above. They correspond to the central β-sheet, which is treated as a single structural entity, and the surrounding four α-helices. RDC's from residues 92, 177−179, and 190 were omitted from the analysis as the corresponding residues were not found to be in a β conformation in the model structure. The magnitudes of the alignment tensors for the individual domains are similar, and the orientations of the tensor axes are found to be almost coaxial relative to the common molecular frame (Figure 5A). This provides strong evidence that the relative orientation of the α-helices and β-sheet in the homology-based model of SiR-FP18 is similar to that found in solution, an observation confirmed by the analysis of these elements as one structural domain, which also shows close agreement between calculated and experimental couplings (Figure 5B−D).

Having verified that the overall fold of the initial model is in agreement with independently measured RDC's, and therefore probably representative of the solution structure, we have refined the conformation using all of the measured experimental NMR data, i.e., secondary structure restraints and RDC's. To avoid the translational shift of secondary structural elements during the calculation, the global topology is weakly tethered to the initial model topology. The backbone rmsd of the lowest energy structures from the repeated calculations compared to the mean coordinates was 1.3 ± 0.2 Å. The ensemble derived from the control calculation, identical except for the absence of RDC data, refined to an rmsd over the backbone of 3.2 ± 0.5 Å over the ensemble. The lowest energy conformer from the RDC refinement is shown in Figure 6; this has a backbone rmsd of 1.9 Å compared to the initial structural model. It can be seen that the typical flavodoxin-like fold is well conserved. The rmsd compared to human CPR and P450-BM3, taken again over the backbone atoms of the secondary structure elements, is 1.98 and 1.95 Å, respectively.

DISCUSSION

The crystal structure of SiR-FP60, the monomeric model of the flavoprotein component of the *E. coli* sulfite reductase, has been previously determined (*14*). However, the first 172 N-terminal amino acid residues (residues 52−224), corresponding to the flavodoxin-like domain, were not defined in any of the electron density maps obtained. To complete the crystal structure of the flavoprotein component, we have now expressed a protein corresponding to residues 52−219, called SiR-FP18 with respect to its theoretical molecular mass of 17 870 Da. The choice of the domain borders was guided by previous results from limited proteolysis of SiR-FP60, during which an analogous fragment had been obtained (*12*).

SiR-FP18 was purified as a monomeric, partially depleted FMN-containing protein. Reconstitution could only be achieved with FMN, demonstrating its selectivity toward the naturally bound flavin. Its photoreduction in the presence of deazaflavin−EDTA proceeded in two distinct steps with accumulation of the one-electron-reduced form $FMNH^\bullet$ before full reduction to the hydroquinone form ($FMNH_2$). The $FMNH^\bullet$ form of the protein can be defined as the air-stable semiquinone form of the protein since it is generated immediately after air admission on the anaerobically fully reduced SiR-FP18. These results suggest a strong conservation in SiR-FP18 of the difference between the midpoint potential of the $FMNH^\bullet$/FMN couple (−130 ± 10 mV) and the $FMNH_2$/$FMNH^\bullet$ couple (−335 ± 10 mV) previously determined in SiR-FP23 (*15*). The 200 mV difference between these two couples explains the high degree of thermodynamic stabilization of the $FMNH^\bullet$ radical SiR-FP18, either under the semiquinone or under the hydroquinone

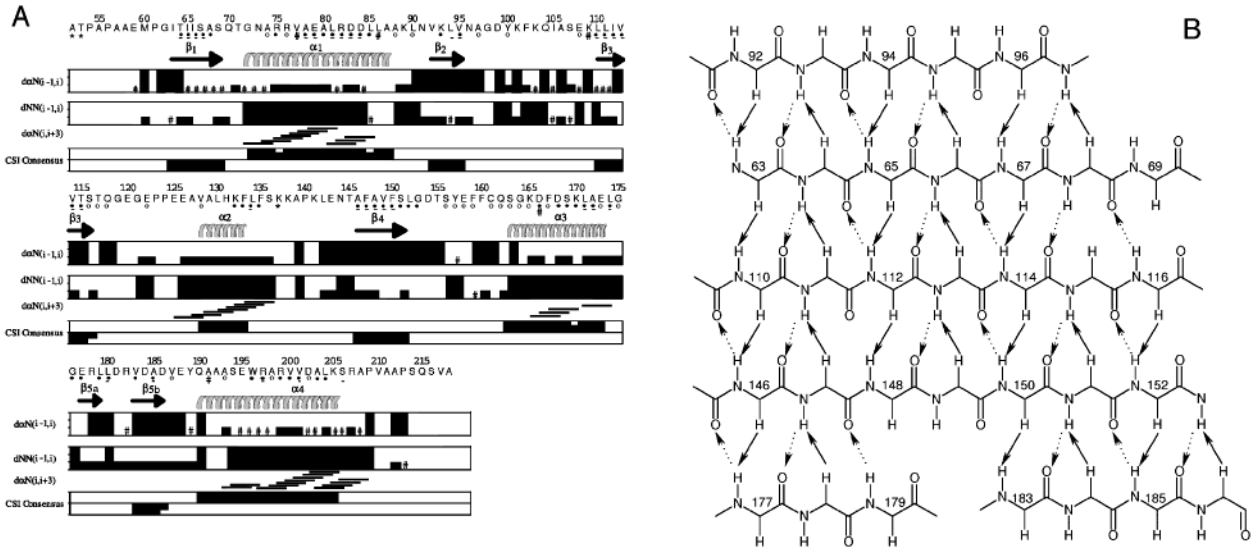

FIGURE 4: Secondary structure information obtained from NMR. (A) Amide protons protected from solvent exchange for 15 min, 12 h, and 1 month are represented respectively by (○), (●), and (_); sequential and intraresidue NOEs are indicated by black bars, where the height corresponds to the intensity (#, NOEs not observed because of resonance overlap; *, missing assignments); positive and negative values of the consensus chemical shift index are indicative for α-helices and β-strands, respectively. (B) Schematic representation of the NOEs and hydrogen bonds used to deduce the topology of the β-sheet. H^N-H^α NOEs are shown as arrows; dashed arrows represent hydrogen bonds as identified by scalar $^{3h}J_{NC'}$ couplings.

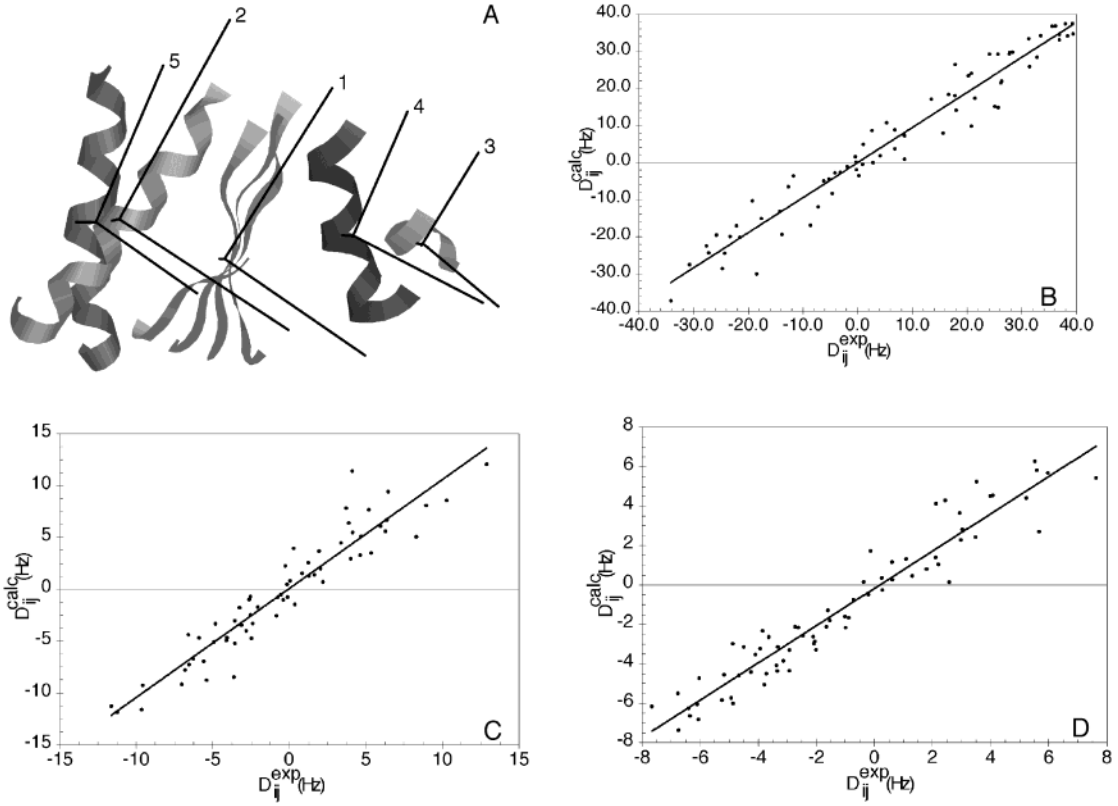

FIGURE 5: Model refinement using the program MODULE. (A) Relative orientation of the five different secondary structure elements in the SWISS-MODEL structure and their associated alignment tensors. Secondary structure elements are defined in the text. Numbers from 1 to 5 correspond to the central β-sheet and helices I, II, III, and IV, respectively. The amplitude of the axes shown corresponds to the eigenvalues of the alignment tensors. The axial and rhombic components as well as the total reduced χ^2 of the five secondary structure elements are as follows: 1, $A_a = 16.07e^{-4}$, $A_r = 10.53e^{-4}$, $\chi^2 = 9.7$; 2, $A_a = 17.62e^{-4}$, $A_r = 10.50e^{-4}$, $\chi^2 = 7.5$; 3, $A_a = 16.89e^{-4}$, $A_r = 10.49e^{-4}$, $\chi^2 = 1.1$; 4, $A_a = 18.54e^{-4}$, $A_r = 9.09e^{-4}$, $\chi^2 = 6.6$; 5, $A_a = 16.82e^{-4}$, $A_r = 6.99e^{-4}$, $\chi^2 = 9.0$. (B−D) Correlation plots between D_{ij}^{exp} and $D_{ij}^{backcal}$ for $^1D_{NH}$ (B), $^1D_{C'HN}$ (C), and $^1D_{C'C\alpha}$ (D). The five different secondary structure elements were fitted as a single entity. The axial and rhombic components and the total reduced χ^2 are $A_a = 17.47e^{-4}$, $A_r = 11.37e^{-4}$, and $\chi^2 = 9.1$.

form, could be fully oxidized by DCPIP, ferricytochrome *c*, or ferricyanide. The reaction, quantified here using DCPIP, was fast and quantitative. It should be noticed that $FMNH_2$ gives its two electrons to DCPIP without the detectable transient appearance of $FMNH^\bullet$. The overall reactivity of SiR-FP18 was thus very similar to that of SiR-FP23, showing

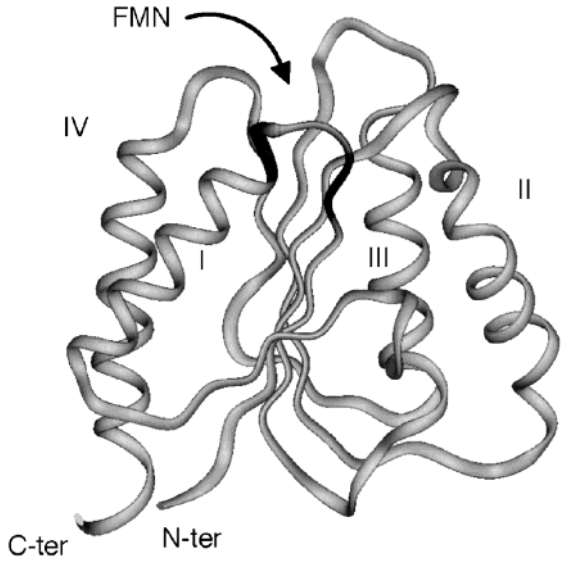

FIGURE 6: Three-dimensional structure of SiR-FP18 after refinement using Sculptor. The backbone of SiR-FP18 is shown in ribbon representation; Roman numerals designate the four α-helices. Residues situated close to the presumed FMN-binding site (arrow) and whose amide protons are shifted above 9.5 ppm are darkened.

that this monomeric fragment is a good model of its polymeric counterpart.

We had previously shown that SiR-FP and SiR-FP60 interact strongly with cytochrome P450c17 in vitro but only SiR-FP could transfer electrons to this artificial partner (*32*). This was interpreted as a requirement of the N-terminal part of the protein in the electron-transfer process. With the hemoprotein component of SiR as the electron acceptor, both a very tight interaction and electron transfer were possible from SiR-FP60 (*13*). We have demonstrated now that it is also the case with SiR-FP18, although these latter proteins missed the first 51 amino acids. Interestingly, only the fully reduced form of SiR-FP18 was able to transfer one electron to SiR-HP, generating the one-electron-reduced form of the flavoprotein ($FMNH^{\bullet}$). This resulted also in the reduction of the ferrisiroheme as judged from the almost complete disappearance of its EPR signal. In the equilibrium state so obtained, a small part of the siroheme signal, estimated at about one-third of the original one, persisted along with the signal of the FMN semiquinone. The addition of sulfite, the natural substrate of the protein, only led to the disappearance of the remaining heme signal, the FMN semiquinone signal being stable. It has been shown that the complex between reduced SiR-HP and SO_3^{2-} was stable under anaerobic conditions (*33*) and that sulfite could be reduced only if additional reducing equivalents became available. In other words, under these conditions, sulfite could not oxidize reduced SiR-HP in the absence of an external reductant at a lower potential than $FMNH^{\bullet}$. It has also been shown that oxidized SiR-HP could slowly form an EPR-silent complex with sulfite (*33*) whose nature is unclear. However, in the present study, the remaining heme signal disappears almost instantaneously upon addition of SO_3^{2-}, probably because the thermodynamic equilibrium resulting from the distribution of the electrons after reaction of fully reduced SiR-FP18 with SiR-HP is shifted by the presence of sulfite, thus allowing the complete reduction of the siroheme.

From these experiments, it became clear that SiR-HP can only accept one electron from fully reduced SiR-FP18 although one more electron could theoretically be transferred to the iron−sulfur cluster. However, the EPR signal of a $S = 1/2$ $(Fe_4S_4)^{+1}$ cluster was never observed during these experiments. This is consistent with the hypothesis that in SiR-FP, the FMN cofactor cycles between the hydroquinone and the semiquinone forms (*34*), as already demonstrated with the homologous protein CPR (*35*). This can also be justified by the E'_m values of the different moieties present in the electron-transfer complex [FMN couples, see above; $(Fe_4S_4)^{+1}/(Fe_4S_4)^{+2} = -405$ mV; ferrosiroheme/ferrisiroheme $= -340$ mV (*36*, *37*)]. A distribution of the electrons between the heme and the FMN is thus plausible with the iron−sulfur cluster serving either as a relay between $FMNH_2$ and ferriheme or as a barrier between $FMNH^{\bullet}$ and the active site. The massive addition of sulfite triggered the full reduction of the heme but not of the iron−sulfur cluster as the quantity of FMN semiquinone was not significantly changed. To be catalytically active in SiR-FP, $FMNH^{\bullet}$ must be reduced to $FMNH_2$ very likely by $FADH_2$ that, in turn, must oxidize to $FADH^{\bullet}$. The presence of the one-electron-reduced form of the FAD moiety has never been detected during steady-state or stopped-flow analyses of SiR-FP (*34*), very likely because of its extreme reactivity and instability. However, using the isolated FAD-binding domain (*12*, *38*), we have previously demonstrated that the FAD semiquinone state could exist and was stable enough to be detected during air oxidation of anaerobically fully reduced $FADH_2$.

We then were interested in the reasons for the absence of the electron density of the flavodoxin-like domain of SiR-FP60 (*14*). In the NMR experiments, SiR-FP18 appears as a properly folded, stable protein. The ^1H,^{15}N correlation spectrum of SiR-FP18 was found to be very well dispersed (*31*), and no indication could be obtained from the ^1H and ^{15}N chemical shift data concerning significant chemical exchange or the presence of unstructured regions, even in the absence of FMN. Interstrand distances and hydrogen bonds were detected for the entire central β-sheet, indicating a high structural stability. These observations suggest that the absence of the electron density in the previous crystal study of the entire flavoprotein could be explained by the motion of the flavodoxin-like domain with respect to the rest of SiR-FP60. An analogous behavior has also been suggested in the case of the eukaryotic cytochrome P450 reductase. Using site-directed mutagenesis, residues involved in electron transfer to cytochrome P450 have been identified (*17*). However, the same structural region was covered by the FAD of the FAD/NADPH-binding domain in the crystal structure of the entire rat CPR (*16*). Consequently, it was suggested that the binding of cytochrome P450 requires a movement of the FMN-binding domain facilitated by the presence of the flexible linker between this domain and the rest of the molecule (*17*). Identical results have very recently been reported on the homologous bacterial electron-transfer system formed of ferredoxin−$NADP^+$ reductase, flavodoxin, and cobalamin-dependent methionine synthase (*39*). NMR chemical shift mapping was used to show that both physiological partners bind to overlapping sites on flavodoxin, indicating again the need for relative domain−domain reorientation during the electron-transfer reaction.

The final aim of the NMR study of SiR-FP18 is the completion of the high-resolution structure of SiR-FP as well as the investigation of the electron-transfer complex with the hemoprotein (β-subunit). However, at the present state of the work, we can use the information provided by NMR to propose a low-resolution model of SiR-FP18 based on sequence similarity considerations and validated by experimental NMR data. It has been proposed that *E. coli* sulfite reductase, CPR, nitric oxide synthase, and P450-BM3 share a common fold (*16*). The initial structure prediction process was therefore based on a combination of experimentally identified secondary structural elements and the high-resolution crystallographic structures of homologous molecules, the flavodoxin-like domains of human CPR and P450-BM3. These two domains show 29% and 26% sequence identity with SiR-FP18, respectively, and could be used as templates. The resulting model was further validated by independently obtained experimental RDC data. Using the program MODULE, the model was shown to be in very good agreement with measured RDC data, both with respect to the relative orientation of the previously identified secondary structure elements in the model and with respect to the effective alignment experienced by each individual element (Figure 5). The final structural model, comprising residues 60−210, was refined in the presence of all of the measured experimental NMR data (Figure 6). As expected, the relative orientation of the secondary structural elements does not change significantly during the calculation. Helix 2 is tilted slightly under the influence of the RDC data, while the C-terminal helix is less curved. Interestingly, region 96−100, an extended loop in the model structure, is also found to fold into a single helical turn due to the RDC restraints.

Some features in the C-terminal part of the molecule merit further discussion. In CPR but not in P450-BM3, there is a small supplementary β-strand, named 5a, which is nearly perpendicular to the other strands but is connected by three hydrogen bonds to β-strand 4. These hydrogen bonds are absent in the P450-BM3 structure. In the case of SiR-FP18, the analogous hydrogen bonds have been identified in the long-range, cross hydrogen bond HNCO experiment and are also present in the refined structure of SiR-FP18. The dihedral angles of residues 177−179 are very close to those found in β-strand 5a in CPR. In addition, the analysis of the SWISS-MODEL structure revealed some ambiguities at the level of the loop connecting the fifth β-strand and the C-terminal helix. In the SiR-FP18 sequence, there is a two-residue deletion presumably in the loop region. Depending on the position of these two deletions, either the β-strand or the α-helix of the SWISS-MODEL structure agrees less well with the RDC data than the rest of the molecule. This indicates that the local structure is slightly different from the model structure. This is confirmed in the refined structure, where a change of conformation occurs in the short β-loop between the final strand of the β-sheet and the C-terminal helix, resulting in a slight shift of the position of the helix. It should be noted that this treatment of the available experimental data only allows us to judge the correctness of the backbone conformation of the SiR-FP18 model, and to refine this model. More detailed studies using NOE data or RDC's measured on side-chain atoms are necessary in order to obtain a high-resolution structure of SiR-FP18.

As expected, SiR-FP18 shows the same fold as bacterial flavodoxins which also possess an FMN as cofactor. At the present state of the work, no attempts were made to identify the exact localization of the prosthetic group in the protein. However, in bacterial flavodoxins as well as in human CPR, the amide proton chemical shifts in the phosphate-binding loop are shifted to low-field (*40*, *41*). A very analogous behavior is observed in the present study where the amide protons of S69, Q70, N73, and A74 are found between 9.5 and 11.5 ppm. These results confirm the structural conservation of FMN binding already suggested by the selective binding of FMN by SiR-FP18. A further key feature of FMN binding is the conservation of two aromatic residues which flank the isoalloxazine ring (Y80 and Y118 in human CPR and Y536 and W574 in P450-BM3, crystal structure numbering). However, in the sequence of SiR-FP18, the first of these residues is not conserved and replaced by a glutamine. A more detailed structural analysis is needed to elucidate the binding of FMN in the case of SiR-FP18.

ACKNOWLEDGMENT

We are grateful to Accelrys Inc. for continuing collaboration. We thank Dr. Stéphane Ménage for his help during EPR experiments and David Lascoux for the determination of the exact mass of the protein.

REFERENCES

1. Kredich, N. M. (1996) in *Escherichia coli and Salmonella thyphimurium: Cellular and Molecular Biology* (Neidhard et al., Eds.) pp 514−527, ASM Press, Washington, DC.
2. Siegel, L. M., and Davis, P. S. (1974) *J. Biol. Chem. 249*, 1587−1598.
3. Eschenbrenner, M., Covès, J., and Fontecave, M. (1995) *J. Biol. Chem. 270*, 20550−20555.
4. Eschenbrenner, M., Covès, J., and Fontecave, M. (1995) *FEBS Lett. 374*, 82−84.
5. Karplus, P. A., and Bruns, C. M. (1994) *J. Bioenerg. Biomembr. 26*, 89−99.
6. Porter, T. D., and Kasper, C. B. (1986) *Biochemistry 25*, 1682−1687.
7. Bredt, D. S., Hwang, P. M., Glatt, C. E., Lowenstein, C., Reed, R. R., and Snyder, S. H. (1991) *Nature 351*, 714−718.
8. Siegel, L. M., Davis, P. S., and Kamin, H. (1974) *J. Biol. Chem. 249*, 1572−1586.
9. Ostrowski, J., Barber, M. J., Rueger, D. C., Miller, B. E., Siegel, L. M., and Kredich, N. M. (1989) *J. Biol. Chem. 264*, 15796−15808.
10. Crane, B. R., Siegel, L. M., and Getzoff, E. D. (1995) *Science 270*, 59−67.
11. Covès, J., Zeghouf, M., and Fontecave, M. (2000) *Recent Res. Dev. Biochem. 2*, 97−107.
12. Zeghouf, M., Fontecave, M., Macherel, D., and Covès, J. (1998) *Biochemistry 37*, 6114−6123.
13. Zeghouf, M., Fontecave, M., and Covès, J. (2000) *J. Biol. Chem. 275*, 37651−37656.
14. Gruez, A., Pignol, D., Zeghouf, M., Covès, J., Fontecave, M., Ferrer, J. L., and Fontecilla-Camps, J. C. (2000) *J. Mol. Biol. 299*, 199−212.
15. Covès, J., Zeghouf, M., Macherel, D., Guigliarelli, B., Asso, M., and Fontecave, M. (1997) *Biochemistry 36*, 5921−5928.
16. Wang, M., Roberts, D. L., Paschke, R., Shea, T. M., Masters, B. S., and Kim, J. J. (1997) *Proc. Natl. Acad. Sci. U.S.A. 94*, 8411−8416.
17. Zhao, Q., Modi, S., Smith, G., Paine, M., McDonagh, P. D., Wolf, C. R., Tew, D., Lian, L. Y., Roberts, G. C., and Driessen, H. P. (1999) *Protein Sci. 8*, 298−306.

18. Sevrioukova, I. F., Li, H., Zhang, H., Peterson, J. A., and Poulos, T. L. (1999) *Proc. Natl. Acad. Sci. U.S.A. 96*, 1863−1868.
19. Jansson, M., Li, Y. C., Jendeberg, L., Anderson, S., Montelione, B. T., and Nilsson, B. (1996) *J. Biomol. NMR 7*, 131−141.
20. Bradford, M. M. (1976) *Anal. Biochem. 72*, 248−254.
21. Laemmli, U. K. (1970) *Nature 227*, 680−685.
22. Whitby, L. G. (1953) *Biochem. J. 53*, 437−442.
23. Cordier, F., and Grzesiek, S. (1999) *J. Am. Chem. Soc. 121*, 1601−1602.
24. Yang, D., Venters, R. A., Mueller, G. A., Choy, W. Y., and Kay, L. E. (1999) *J. Biomol. NMR 14*, 333−343.
25. Brutscher, B. (2001) *J. Magn. Reson. 151*, 332−338.
26. Guex, N., and Peitsch, M. C. (1997) *Electrophoresis 18*, 2714−2723.
27. Wishart, D. S., and Sykes, B. D. (1994) *J. Biomol. NMR 4*, 171−180.
28. Dosset, P., Hus, J. C., Marion, D., and Blackledge, M. (2001) *J. Biomol. NMR 20*, 223−231.
29. Hus, J. C., Marion, D., and Blackledge, M. (2000) *J. Mol. Biol. 298*, 927−936.
30. Sibille, N., Pardi, A., Simorre, J. P., and Blackledge, M. (2001) *J. Am. Chem. Soc. 49*, 12135−12146.
31. Sibille, N., Covès, J., Marion, D., Brutscher, B., and Bersch, B. (2001) *J. Biomol. NMR 21*, 71−72.
32. Zeghouf, M., Defaye, G., Fontecave, M., and Covès, J. (1998) *Biochem. Biophys. Res. Commun. 246*, 602−605.
33. Janick, P. A., and Siegel, L. M. (1983) *Biochemistry 22*, 504−515.
34. Siegel, L. M., Faeder, E. J., and Kamin, H. (1972) *Z. Naturforsch., B 27*, 1087−1089.
35. Vermilion, J. L., Ballou, D. P., Massey, V., and Coon, M. J. (1981) *J. Biol. Chem. 256*, 266−277.
36. Janick, P. A., and Siegel, L. M. (1982) *Biochemistry 21*, 3538−3547.
37. Siegel, L. M., Rueger, D. C., Barber, M. J., Krueger, R. J., Orme-Johnson, N. R., and Orme-Johnson, W. H. (1982) *J. Biol. Chem. 257*, 6343−6350.
38. Covès, J., Lebrun, C., Gervasi, G., Dalbon, P., and Fontecave, M. (1999) *Biochem. J. 342*, 465−472.
39. Hall, D. A., Vander Kooi, C. W., Stasik, C. N., Stevens, S. Y., Zuiderweg, E. R., and Matthews, R. G. (2001) *Proc. Natl. Acad. Sci. U.S.A. 98*, 9521−9526.
40. Peelen, S., Wijmenga, S., Erbel, P. J., Robson, R. L., Eady, R. R., and Vervoort, J. (1996) *J. Biomol. NMR 7*, 315−330.
41. Barsukov, I., Modi, S., Lian, L. Y., Sze, K. H., Paine, M. J., Wolf, C. R., and Roberts, G. C. (1997) *J. Biomol. NMR 10*, 63−75.

BI016008I